CNN-BASED ON-BOARD INTERFERENCE DETECTION IN SATELLITE SYSTEMS: AN ANALYSIS OF DATASET IMPACT ON PERFORMANCE

Saed Daoud Geoffrey Eappen Flor Ortiz Eva Lagunas Wallace Martins Symeon Chatzinotas

University of Luxembourg
Interdisciplinary Centre for Security, Reliability and Trust (SnT)
L-1855, Luxembourg

ABSTRACT

Flying satellite communication systems often have to deal with intended and unintended radio-frequency interference, especially now with the advent of non-geostationary orbit (NGSO) systems causing orbital crowding. In this work, we investigate the use of machine learning (ML) for interference detection and classification. In particular, we investigate the effects of datasets representations on the performance of convolutional neural network (CNN) when deployed on-board of a geostationary orbit (GSO) satellite, to detect interference and classify the spectrum of interest. Focusing on the frequency representation of the observed signal, we consider different input datasets depending on the fast Fourier Transform (FFT) size and their transformation. In particular, we considered complex and magnitude values of full dimension and reduced dimension FFT. Our analysis shows that the magnitude of the reduced dimension FFT, attains the best results in terms of accuracy in detecting the presence of the interference signal, and its location in the spectrum of interest.

Index Terms— convolutional neural network, fast Fourier transform, interference detection, satellite communication

1. INTRODUCTION

The development of non-geostationary (NGSO) satellite technology, has led or will soon lead to an increase in the number of satellites in space [1,2]. Competing for the same spectrum, interference becomes a crucial problem in satellite communication (SATCOM). According to [3], 93% of satellite operators suffer from interference at least once a year, and more than half experience it monthly. An important step before tackling interference is to detect it and understand which part of the spectrum it is affecting.

This research was partially funded by the Luxembourg National Research Fund (FNR) under the project SmartSpace (C21/IS/16193290).

An energy-based on-board satellite interference detector was proposed in [4, 5]. In particular, the authors considered the energy detection (ED) technique, to decide whether an interference is present or not. An alternative approach is proposed in [6], where compressive sensing is used to estimate the power spectrum of the signal. Other works focus on the localization of interference by using time-difference of arrival or frequency difference of arrival, e.g. [7].

Recently, machine learning (ML)-based solutions on SATCOM are gathering attention due to its real-time capability in performing complex operations [8, 9], for example, to automatically detect interference in the spectrum of the received signal. Furthermore, the ML model can be trained on sample data offline, and the resulting model to detect interference can be deployed online. This shifts the complexity and processing from online to offline, which reduces the decision time online [10]. In addition, one ML model can detect different interference signals. This reduces the number of units needed to detect several interference signals.

The most relevant SATCOM ML-related work is [11], where a long short-term memory (LSTM) tool is implemented to predict the expected signal snapshot and compare it with the actual one. More recently, [12] investigated the use of deep learning (autoencoder) for on-ground terrestrial-to-satellite terminal interference detection. In [13], the authors studied the general problem of wireless signal identification, which covers the problems of modulation recognition, as well as interference identification, using ML algorithms.

In this paper, we address the problem of interference detection and its location within the spectrum of interest by casting it as a classification ML problem. Our main goal is to study the impact of the input dataset format and feature space dimension on the performance of the ML model for on-board interference detection and spectrum classification. To this end, we consider a geosynchronous orbit (GSO) and non-geosynchronous orbit (NGSO) satellite systems operating over the same spectrum in the uplink of the return link, where the total available spectrum is divided into a number of nonoverlapping subbands, and at any given time the GSO and NGSO system (if transmitting) can use only one

subband. The GSO system employs a convolutional neural network (CNN) that operates on the pre-processed analog-to-digital (A/D) converter samples in the frequency domain, to decide whether there is interference in the currently operated subband by the GSO satellite or not, in order to eventually decide whether or not to change the carrier frequency to a subband that is interference-free. Since we are interested in detecting interference and classifying the spectrum using the same model, different fast Fourier transform (FFT) frequency representations and sizes of the A/D samples are considered and evaluated.

The rest of the paper is organized as follows: in Section 2, the system and signal models are presented. In Section 3, the details of the data generation process of the different representations are outlined. In Section 4, the CNN architecture is provided. In Section 5, the CNN classification accuracy on the different data representations are evaluated, and in Section 6, a conclusion is discussed.

2. SYSTEM AND SIGNAL MODEL

In the uplink of a GSO system return link, a GSO source $\mathtt{S_D}$ and an NGSO source $\mathtt{S_I}$ are transmitting the baseband signals $x_{\rm d}(t)$ and $x_{\rm i}(t)$, henceforth called the desired and interference signals, respectively. These signals are given by

$$x_{\rm z}(t) = \sum_{k=0}^{K-1} x_{\rm z}[k]\, g\left(t - kT\right), \;\; t \in [0, KT] \tag{1}$$

where $\{x_z[k]\}_{k=0}^{K-1}$ are modulated symbols drawn from a binary phase shift keying (BPSK) constellation for ${\rm z} \in \{{\rm d}, {\rm i}\}$, each with unity power and duration T, $g(t)$ is a rectangular pulse shaping filter of duration T and unit energy. T is related to the baseband bandwidth of the signals W as $T = \frac{1}{W}$, and K is the number of symbols in the transmitted block. We assume that the spectrum range $[f_{\rm min},\, f_{\rm max}]$ is allocated to the GSO satellite system, which is divided into V nonoverlapping subbands, each of bandwidth $2W$, i.e., $f_{\rm max} - f_{\rm min} = 2VW$, where $V \in \mathbb{Z}^+$. Each subband $\mathcal{D}_v$ has a center frequency $\mathcal{F}_v$ for $v = 1, 2, \cdots, V$. The carrier frequency of the desired signal $f_{\rm d}$ can assume any of these center frequencies and subbands. At the beginning, it is assumed that $f_{\rm d} = \mathcal{F}_1$, i.e., $x_{\rm d}(t)$ occupies the first subband, which can change whenever the first subband suffers from a significant interference that disturbs the quality-of-service (QoS) of the desired signal transmission.

At the receiver $\mathtt{R}$, which is the GSO satellite, the baseband received signal can be expressed in the time-domain, after down-converting the bandpass received signal by frequency $f_{\rm d}$ as

$$r(t) = x_{\rm d}(t)\sqrt{\mathtt{SNR_d}} + \alpha\, x_{\rm i}(t) e^{j2\pi(f_{\rm i} - f_{\rm d})t}\sqrt{\mathtt{SNR_i}} + n(t) \tag{2}$$

where $f_{\rm d}$ is the carrier frequency of the signal $x_{\rm d}(t)$, $f_{\rm i} \in \mathcal{F} = \{\mathcal{F}_1, \mathcal{F}_2, \mathcal{F}_3, \cdots, \mathcal{F}_V\}$ is the carrier frequency of the signal $x_{\rm i}(t)$, and $n(t)$ is complex-valued additive white Gaussian noise (AWGN) process of zero-mean and unity power over the bandwidth $2W$. $\mathtt{SNR_d}$ and $\mathtt{SNR_i}$ are the signal-to-noise ratio (SNR) of the signals $x_{\rm d}(t)$ and $x_{\rm i}(t)$, respectively, over a bandwidth of $2W$. The variable $\alpha \in \{0, 1\}$ indicates the presence or absence of the interference signal $x_{\rm i}(t)$. At the analog-to-digital (A/D) converter at the GSO satellite, the baseband received signal is sampled by a sampling frequency $f_s = 1/T_s$ Hz, where T_s is the sample time.

2.1. Interference Detection and Spectrum Classification

To classify the subbands in the spectrum $[f_{\rm min},\, f_{\rm max}]$ as containing interference or not, we need first to define a metric that determines if a subband contains a significant interference to disturb the QoS of the GSO system or not. We adopt the maximum bit error rate (BER) metric denoted by ε and the corresponding minimum SINR denoted by $\mathtt{SINR_{min}}$ that must be satisfied to meet the QoS of the desired signal. Mathematically

$$\varepsilon = Q\left(\sqrt{2\,\mathtt{SINR_{min}}}\right) \tag{3}$$

or, equivalently

$$\mathtt{SINR_{min}} = \frac{\left[Q^{-1}\left(\varepsilon\right)\right]^2}{2} = \frac{\mathtt{SNR_d}}{\mathtt{SNR_{i,max}} + 1} \tag{4}$$

where $Q(.)$ and $Q^{-1}(.)$ are the Q and inverse-Q functions, respectively. The maximum allowed interference from $\mathtt{S_I}$ at $\mathtt{R}$ is denoted by $\mathtt{SNR_{i,max}}$ and can be found from (4) as

$$\mathtt{SNR_{i,max}} = \max\left(\frac{\mathtt{SNR_d}}{\mathtt{SINR_{min}}} - 1,\, 0\right) \tag{5}$$

3. GENERATING THE DATA

In this section, we explain the process of generating the data. We consider full-dimension and reduced-dimension FFT, where for each case we considered the complex FFT, and magnitude FFT, which results in a total of four datasets that will be evaluated and compared. For all cases, we consider the following fixed parameters: $f_{\rm d} = 29.55$ GHz, $W = 50$ MHz, $f_s = 5$ GHz, $K = 10$, $\mathtt{SNR_d} = 12$ dB, $\mathtt{SNR_i} = 6$ dB, $\varepsilon = 10^{-5}$. The interference signal's carrier frequency takes on the values

$$\mathcal{F}_{\rm i} = \{A | A = 29.55,\, 29.65,\, 29.75,\, 29.85,\, 29.95\} \;\; \text{GHz} \tag{6}$$

The input data are the complex/magnitude FFT of the received signal, and the output data is 5-binary-valued vectors, where each binary digit indicates the presence or absence of the interference in the corresponding subband. As a result we have 6 classes, which correspond to the cases for no interference in any subband, or the presence of interference in one of the subbands.

For each input data dimension size/representation, for example, full-dimension/complex FFT representation, we generated 2500 data points per class, which are then divided into 80% training, and 20% validation data. For complex FFT, the input data is pre-processed as explained in Section 5.1, while for magnitude FFT, we take the magnitude of the FFT transformation.

3.1. Full Dimension FFT

At the output of the A/D converter, the bandwidth of the FFT of the signal spans the spectrum $\left(-\frac{fs}{2}, \frac{fs}{2}\right]$, and the number of frequency bins in the frequency domain equals to the number of samples in the time domain, which is $S = 1000$. In this case the training datasets has dimensions of 12000×1000, and the validation datasets has a dimension of 3000×1000.

3.2. Reduced-Size FFT

Although the FFT signal bandwidth covers the spectrum $\left(-\frac{f_s}{2}, \frac{fs}{2}\right]$ in baseband, most of this spectrum falls outside the spectrum of interest, which spans the spectrum $[-W, 9W]$. Thus, before preparing the data, we extract the part of FFT that corresponds to the spectrum of interest, and this results in $U = 100$ frequency bins in the frequency domain in this spectrum. In this case the training datasets has dimensions of 12000×100, and the validation datasets has a dimension of 3000×100.

4. CNN NETWORK ARCHITECTURE

The Keras-based Sequential CNN model is considered for interference detection and spectrum classification. The CNN employs the convolution method for the learning operation, therefore it has fewer training parameters as compared to the artificial neural network [14]. The employed CNN model comprises a convolutional input layer with a rectified linear unit (ReLU) as an activation function. The employed CNN comprises of two convolutional layers with a ReLU activation function followed by the max pool layer in the beginning. The ReLU can be defined as [15]

$$f\left(x^L\right) = \max\left\{0, x^L\right\} = \begin{cases} x^L, & x^L \geq 0 \\ 0, & \text{else} \end{cases} \tag{7}$$

here x^L is the element wise output for the L^{th} layer of the CNN model. The dropout of the proposed CNN model is set to 20%. The same pattern is followed post-dropout but with higher feature maps. Towards the end, CNN comprises flatten layer followed by the fully connected output layer.

The combination of two-dimensional convolutional layers with gradually decreasing feature maps and max pool layer of size 1×1 is continued until feature maps of the convolutional layer reach 4. The intention of the max pooling layer is to reduce the size of the spatial filters and network parameters [16]. This is followed by the flattened layer and fully connected layer with 6 units. The fully connected output layer has a softmax-based activation function as

$$\mathbf{x} = [x_1, \cdots, x_m]^T = \sigma(\mathbf{h}) \tag{8}$$

here, x_m is the predicted interference showing the m^{th} value in the M classes. The $\mathbf{h} = [h_1, \cdots, h_M]^T$ is the final output from the fully connected layer. The softmax function $\sigma(\mathbf{h})$ is evaluated as

$$x_m = [\sigma(\mathbf{h})]_m = \frac{e^{h_m}}{\sum_{i=1}^{M} e^{h_i}} \tag{9}$$

4.1. CNN Architecture: Full Dimension FFT

The training data shape is (12000, 1, 1000, 1) and the validation data shape is (3000, 1, 1000, 1). The convolutional 2D (Conv2D) layer has 100 filters with (1,1) as the kernel. The input data shape to which convolutional filters are applied is (1, 1000,1). Post extracting the features, the output shape has the dimension (None, 1, 1000, 100), here 1000 is the number of rows in the output feature map, 100 is the number of columns, and 1 is the number of filters. This layer has 200 trainable parameters.

4.2. CNN Architecture: Reduced Size FFT

The first Conv2D layer has 100 filters and a kernel size of (1,1). This layer applies convolution operations on the input data of shape (1, 100,1) to extract features. The output shape of this layer is (1, 100, 100), where None indicates the number of samples in a batch, 100 is the number of rows in the output feature map, 100 is the number of columns, and 1 is the number of filters. The detailed description of the CNN architecture is shown in Fig. 1.

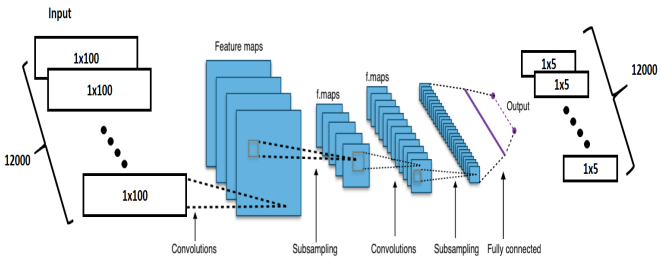

Fig. 1: Convolutional Neural Network for interference detection and spectrum classification

5. PERFORMANCE EVALUATION

The Keras-based CNN model is evaluated based on its prediction accuracy, and training losses. The prediction accuracy is depicted via the confusion matrix. The confusion matrix

is a vital means of understanding neural networks' progress. It comprises true positive and false positive rate. The total number of sub-bands is $V = 5$. Since it is considered that the interference is present in only one sub-band at a time, we have 6 possible classes, which are: $[0\ 0\ 0\ 0\ 0]$, $[1\ 0\ 0\ 0\ 0]$, $[0\ 1\ 0\ 0\ 0]$, $[0\ 0\ 1\ 0\ 0]$, $[0\ 0\ 0\ 1\ 0]$, and $[0\ 0\ 0\ 0\ 1]$. For each class we generated 2000 data points for training, and 500 data points for validation. Class 0 is represented as $[0\ 0\ 0\ 0\ 0]$ indicating no interference, whereas class 1 which is represented by $[0\ 0\ 0\ 0\ 1]$ corresponds to the interference in the 5^{th} sub-band. Similarly, other classes are denoted based on the interference in the respective sub-bands. For example, $[1\ 0\ 0\ 0\ 0]$ indicating the interference in the 1^{st} sub-band. The data set employed for the training is balanced for each class. The model was trained for 15 epochs with a batch size of 100. One of the constraint associated with using CNN model is that the employed architecture is for classifying 6 subbands. For a different number of subbands, the CNN architecture will change based on the input size. The training configuration used the Stochastic Gradient Descent (SGD) optimizer with a learning rate of 0.01, momentum of 0.9 and Nesterov acceleration. The loss function used was the categorical cross-entropy and the model's accuracy was used as the metric.

5.1. Performance evaluation for the full dimension FFT

The performance evaluation for each FFT category is carried out for two different data-set types: complex FFT input and magnitude FFT input. As CNN architecture can not directly take the complex values for the training, the complex FFT input is pre-processed for the training. The pre-processing is done by splitting the complex data into its real and imaginary before feeding it to the proceeding convolutional layers.

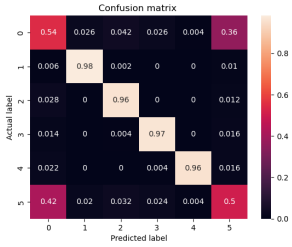

Fig. 2: Full dimension complex FFT

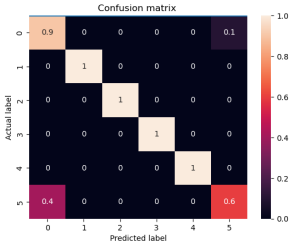

Fig. 3: Full dimension absolute FFT

The classification performance of the CNN architecture is evaluated and depicted via confusion matrix for each data type. The confusion matrix for the full dimension FFT is as shown in Fig. 2 and Fig. 3. It can be inferred from the results that the performance of the CNN model for the full-dimension FFT is better for the magnitude data as compared to the complex data. The difference in performance is because the magnitude data has less correlation between the classes as compared to the complex data.

5.2. Performance evaluation for the reduced size FFT

The CNN model has better performance for the reduced size FFT as compared to the full dimension FFT due to its less correlated classification. In this regard, Fig. 4 and Fig. 5 shows the normalized confusion matrix obtained for the interference detection considering reduced dimension FFT.

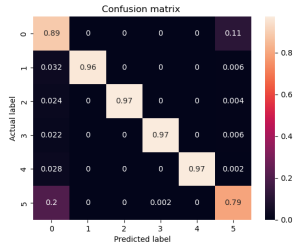

Fig. 4: Reduced dimension complex FFT

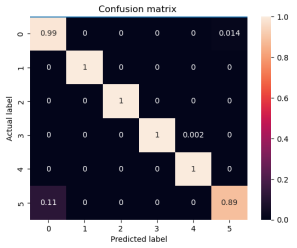

Fig. 5: Reduced dimension absolute FFT

It is observed that for the reduced dimension complex FFT we obtain a ratio higher than 96% in classes 1 to 4, and reach a ratio of 100% for classes 1 to 4 in the case of magnitude values of reduced dimension FFT. A ratio of 100% is the indication that the model is correctly identifying the classes. The employed CNN model has high accuracy in classification for the magnitude values of the full-sized and reduced FFT compared to the complex values. Moreover, the inference from the performance evaluation of the CNN model can be drawn in favor of the reduced FFT for the corresponding representations.

6. CONCLUSION AND FUTURE WORK

In this paper we evaluated the accuracy of a CNN model deployed on-board of a GSO satellite, in the context of interference identification and spectrum classification, using different feature space dimensions and data representations of the FFT of the samples at the output of the A/D converter. The results showed that the magnitude value of the FFT reduced to the bandwidth of interest has the best performance, while reduced size FFT gives better performance than full size FFT for the corresponding data representations, by eliminating the features that are not relevant to the spectrum of interest.

As a future work, we will consider the effect of using different modulation schemes, and SINR values that reflect different NGSO satellite altitudes. We will also study the scalability of the system for any number of subbands and interferers.

7. REFERENCES

[1] R. Li, P. Gu, and C. Hua, "Optimal beam power control for co-existing multibeam geo and leo satellite system," in *2019 11th International Conference on Wireless Communications and Signal Processing (WCSP)*, 2019, pp. 1–6.

[2] O. Kodheli, E. Lagunas, N. Maturo, S. K. Sharma, B. Shankar, J. F. M. Montoya, J. C. M. Duncan, D. Spano, S. Chatzinotas, S. Kisseleff, J. Querol, L. Lei, T. X. Vu, and G. Goussetis, "Satellite communications in the new space era: A survey and future challenges," *IEEE Communications Surveys Tutorials*, vol. 23, no. 1, pp. 70–109, 2021.

[3] "How to Locate and Mitigate Common Satellite Interference Issues, Feb. 2021," https://anritsu.typepad.com/interferencehunting/2021/02/locate-mitigate-common-satellite-interference-issues.html, accessed: 2023-03.

[4] C. Politis, S. Maleki, S. Chatzinotas, and B. Ottersten, "Harmful Interference Threshold and Energy Detector for On-Board Interference Detection," in *Ka and Broadband Communications Conference, Cleveland, Ohio, USA*, Oct. 2016.

[5] C. Politis, S. Maleki, C. Tsinos, S. Chatzinotas, and B. Ottersten, "On-board the satellite interference detection with imperfect signal cancellation," in *2016 IEEE 17th International Workshop on Signal Processing Advances in Wireless Communications (SPAWC)*, 2016, pp. 1–5.

[6] C. Prakash, D. Bhimani, and V. K. Chakka, "Interference detection & filtering in satellite transponder," *International Conference on Communication and Signal Processing, ICCSP 2014 - Proceedings*, pp. 1394–1399, 11 2014.

[7] A. Kalantari, S. Maleki, S. Chatzinotas, and B. Ottersten, "Frequency of arrival-based interference localization using a single satellite," in *2016 8th Advanced Satellite Multimedia Systems Conference and the 14th Signal Processing for Space Communications Workshop (ASMS/SPSC)*, 2016, pp. 1–6.

[8] F. Ortiz, V. Monzon Baeza, L. M. Garces-Socarras, J. A. Vásquez-Peralvo, J. L. Gonzalez, G. Fontanesi, E. Lagunas, J. Querol, and S. Chatzinotas, "Onboard processing in satellite communications using ai accelerators," *Aerospace*, vol. 10, no. 2, 2023. [Online]. Available: https://www.mdpi.com/2226-4310/10/2/101

[9] M. Vázquez, P. Henarejos, I. Pappalardo, E. Grechi, J. Fort, J. C. Gil, and R. M. Lancellotti, "Machine learning for satellite communications operations," *IEEE Communications Magazine*, vol. 59, no. 2, pp. 22–27, 2021.

[10] W. Qin and F. Dovis, "Situational awareness of chirp jamming threats to gnss based on supervised machine learning," *IEEE Trans. Aerosp. Electron. Syst.*, vol. 58, no. 3, pp. 1707–1720, 2022.

[11] L. Pellaco, N. Singh, and J. Jalden, "Spectrum prediction and interference detection for satellite communications," in *Advances in Communications Satellite Systems. Proceedings of the 37th International Communications Satellite Systems Conference (ICSSC-2019)*, 2019, pp. 1–18.

[12] P. Henarejos, M. Vázquez, and A. I. Pérez-Neira, "Deep learning for experimental hybrid terrestrial and satellite interference management," in *2019 IEEE 20th International Workshop on Signal Processing Advances in Wireless Communications (SPAWC)*, 2019, pp. 1–5.

[13] M. Kulin, T. Kazaz, I. Moerman, and E. De Poorter, "End-to-End Learning From Spectrum Data: A Deep Learning Approach for Wireless Signal Identification in Spectrum Monitoring Applications," *IEEE Access*, vol. 6, pp. 18 484–18 501, 2018.

[14] J. Kim, S. Lee, Y.-H. Kim, and S.-C. Kim, "Classification of interference signal for automotive radar systems with convolutional neural network," *IEEE Access*, vol. 8, pp. 176 717–176 727, 2020.

[15] V. Nair and G. E. Hinton, "Rectified linear units improve restricted boltzmann machines," in *Icml*, 2010.

[16] A. Giusti, D. C. Cireşan, J. Masci, L. M. Gambardella, and J. Schmidhuber, "Fast image scanning with deep max-pooling convolutional neural networks," in *2013 IEEE International Conference on Image Processing*. IEEE, 2013, pp. 4034–4038.